Available online at 2019.creative-construction-conference.com/proceedings/

CCC 2019

Proceedings of the Creative Construction Conference (2019) 010

Edited by: Miroslaw J. Skibniewski & Miklos Hajdu

https://doi.org/10.3311/CCC2019-010

Creative Construction Conference 2019, CCC 2019, 29 June - 2 July 2019, Budapest, Hungary

Identification of the interlayer bond between repair overlay and concrete using nondestructive testing, an artificial neural network and principal component analysis

Sławomir Czarnecki[a,]*, Łukasz Sadowski[a], Jerzy Hoła[a]

Wroclaw University of Science and Technology, Faculty of Civil Engineering, Wybrzeże Wyspiańskiego 27, Wrocław 50-370, Poland

Abstract

In construction practice, concrete elements are exposed to adverse environmental influences, and therefore sooner or later require repair. This repair is usually performed by removing the damaged concrete and replacing it with repair overlay. The quality of this repair is evaluated using the destructive pull-off method. In this method, the pull-off adhesion value between the repair overlay and repaired element is measured (f_b). Unfortunately, the disadvantage of this method is local damage of the element at every measuring point. It is therefore reasonable to present a reliable nondestructive method of identifying the interlayer pull-off adhesion value. The article presents the results of experimental research, which indicate that such identification is possible using complementary non-destructive methods and an artificial neural network with principal component analysis.

© 2019 The Authors. Published by Budapest University of Technology and Economics & Diamond Congress Ltd.

Peer-review under responsibility of the scientific committee of the Creative Construction Conference 2019.

Keywords: concrete interlayer bond, adhesion, nondestructive testing, artificial neural network, principal component analysis;

1. Introduction

Concrete structures and elements are exposed to adverse environmental and service influences, which sooner or later cause the destruction of the subsurface concrete. Depending on the type and time of these influences, the thickness of the damaged concrete may even be several dozen millimeters. Repair of the element is then required, which extends the time of its safe exploitation. The repair is very often performed using a special repair mortar, and the element after repair becomes de facto layered [1]. It is known from construction practice that the thickness of the damaged concrete is not usually the same over the entire surface of the element, and therefore the thickness of the repair overlay is not the same. Regardless of how thick this layer is, it is necessary after the repair to perform quality control of the bonding with the repaired element. The measurable value of this bonding is the value of pull-off adhesion f_b, determined in construction practice using the pull-off method.

The pull-off method is used to control the bonding between the repair overlay and the concrete substrate. Apart from the basic advantage of quantifying the value of the pull-off adhesion, it also has a significant disadvantage. This is local damage to the repair overlay that occurs in every measuring area, which then requires a costly and time-consuming repair after completion of the tests. In the case of large-area concrete elements, the number of control (measuring) areas is counted in hundreds, because according to [2], one measurement should be performed at every

*Corresponding author: Author email: slawomir.czarnecki@pwr.edu.pl

3 m^2. It is therefore reasonable to present a non-destructive method of evaluating the interlayer bond between the repair overlay and the repaired element, thereby significantly limiting the above-mentioned disadvantage.

Due to the fact that the pull-off adhesion value f_b is affected by the preparation of the repaired element surface [3, 4], it may be presumed that the parameters describing this surface morphology can be useful for the non-destructive identification of this bonding [5]. These parameters can be obtained, for example, by means of non-destructive testing using the three-dimensional laser scanning method that is carried out on the surface of the layer prepared for repair. In addition, other non-destructive methods may be useful in identifying the bonding between the layers in the repaired concrete elements. Using the acoustic methods [6], it is possible to obtain parameters on the surface of the repair overlay.

Taking the above into consideration, the aim of this paper is to show that the identification of the interlayer bond between a concrete repair overlay of variable thickness with a repaired element (substrate) can be performed using the above-mentioned complementary non-destructive methods and an artificial neural network with principal component analysis.

2. Description of performed tests

The research involved two double-layer model concrete elements marked with Roman numerals I and II, which are shown in Figure 1. They were used to build a research database consisting of parameters that describe the surface morphology of the concrete substrate representing the repaired element, the parameter describing the thickness of the repair overlay, the parameters assessed using acoustic methods on the surface of the repair overlay, and also the pull-off adhesion of the repair overlay and substrate obtained using the pull-off method.

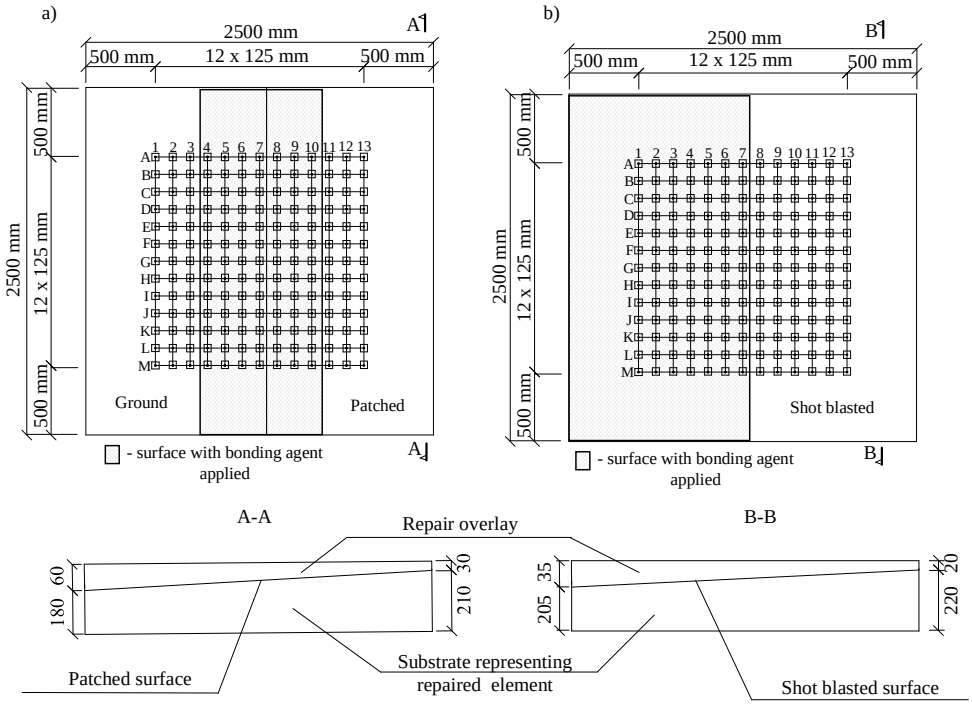

Fig. 1. Scheme of tested elements I (a) and II (b) with the distribution of measuring points

28 days after concreting the substrates of the elements, a grid of 338 measuring areas, 169 for each, was applied on their surfaces, as shown in Figure 1. In these places, tests using geometric leveling were then performed in order to later determine the thickness T of the applied repair overlay. Next, tests describing the morphology of both substrates using the three-dimensional scanning method were performed [7]. The results were obtained as three-dimensional

isometric views of a surface of 50 x 50 mm. Using specialized software, the obtained data was processed and in each of the measuring areas the values of the parameters describing the surface morphology, such as: 10 point height *S10z*, core height *Sk*, reduced peak height *Spk*, 5 point valley height *S5v*, closed hills area *Sha*, density of peaks *Spd*, closed hills volume *Shv*, 5 point peak height *S5p*, and closed dales volume *Sdv* were calculated. The exemplary values of these parameters are given in Table 1.

Table 1. Values of the parameters describing the surface morphology of the substrate.

Lp.	Number of element/ measuring area*	*S10z* [mm]	*Sk* [mm]	*Spk* [mm]	*S5v* [mm]	*Sha* [mm^2]	*Spd* [1/mm^2]	*Shv* [mm^3]	*S5p* [mm]	*Sdv* [mm^3]
1	I/M9	0,623	0,089	0,043	0,299	0,572	1,73	0,0075	0,324	0,0081
2	I/M10	0,857	0,087	0,045	0,312	0,782	1,25	0,0120	0,546	0,0123
3	I/M11	0,856	0,083	0,043	0,515	0,758	1,30	0,0086	0,341	0,0092
4	I/M12	0,677	0,079	0,042	0,296	0,469	2,10	0,0051	0,382	0,0053
					⋮					
337	II/A1	1,900	0,070	0,038	1,170	6,700	0,14	0,1340	0,729	0,0714
338	II/A2	2,270	0,072	0,037	1,440	7,690	0,12	0,1740	0,838	0,0994

* - designation of the measuring point, row and column according to Fig. 1

After applying the bonding agent, the repair overlay was applied on the surface of both elements. Then, after 28 days, a grid of measurement areas with an identical arrangement as on the surface of the substrate was applied on the surface of the repair overlay of both elements. In all of these places of both elements, the thickness of the applied repair overlay T was calculated by means of geometric leveling. Then, after 90 days, , non-destructive tests using impact-echo and impulse response methods were performed in these places, obtaining parameters such as: the frequency relating to the thickness of the element f_T, average mobility N_{av}, dynamic stiffness K_d, voids index v, and mobility slope M_p/N. The exemplary values of the parameters obtained on the repair overlay surface are given in Table 2.

Table 2. Values of the parameters obtained on the repair overlay surface.

Lp.	Number of element/ measuring area *	T [mm]	f_T [kHz]	N_{av} [m/s·N]	K_d [-]	v [-]	M_p/N [-]	f_b [MPa]
1	I/M9	65	8,79	27,3	0,058	0,943	2,580	1,452
2	I/M10	64	8,79	40,4	0,048	1,117	0,636	1,375
3	I/M11	66	8,79	54,6	0,031	0,902	0,358	1,477
4	I/M12	63	6,84	64,3	0,024	1,161	0,465	1,604
				⋮				
337	II/A1	22	8,79	33,3	0,072	0,696	0,777	3,056
338	II/A2	23	8,79	33,2	0,097	0,840	1,191	2,496

* - designation of the measuring point, row and column according to Fig. 1

After performing non-destructive tests, the real pull-off adhesion f_b values were determined in the same measuring areas using the pull-off method. The dataset, including 330 sets of results determined using non-destructive methods and parameter f_b obtained using the pull-off method, was then obtained. Then, in order to identify the value of the pull-off adhesion $f_{c,b}$, numerical analysis was performed. This analysis was performed using the artificial neural network multilayer perceptron [8, 9] with principal component analysis [10, 11].

3. Numerical analysis

The dataset, consisting of parameters obtained based on the experimental tests, was transformed by calculating the C_i components of the principal component analysis. For this purpose, the weights of the dataset parameters are used (w_{11},…, w_{nm}) and the components were determined according to eq. (1), by [11]:

$$C_i = w_{11}(X_1) + w_{11}(X_2) + \cdots + w_{nm}(X_m), \quad (1)$$

where:

X_i – dataset parameter.

It was analysed how the variant transformation of parameters into components C_i of the principal component analysis affects the results obtained by the artificial neural network with the learning algorithm Broyden-Fletcher-Goldfarb-Shano [12] with 10 input parameters and 10 neurons of the hidden layer. Table 3 shows the results of analysis performed for over 40 variants of parameters, which were obtained based on the experimental tests. The results of learning and testing processes of the artificial neural network with principal component analysis, presented as mean values of the linear correlation coefficient *R*, are provided in the table.

Table 3. The results of learning and testing of the artificial neural network with principal component analysis for variants of the used parameters.

Symbols of the used parameters	Linear correlation coefficient value *R* [-] in the learning process	Linear correlation coefficient value *R* [-] in the testing process	Mean linear correlation coefficient value *R* [-] in the learning and testing processes
Spk, Sk, S10z, S5v, Sha, Spd, Shv	0,921	0,871	0,896
Spk, Sk, S10z, S5v, Sha, Spd, Shv, S5p	0,863	0,849	0,856
Spk, Sk, S10z, S5v, Sha, Spd, Shv, S5p, Sdv	0,853	0,843	0,848
Spk, Sk, S10z, S5v, Sha, Spd, T	0,922	0,829	0,876
Spk, Sk, S10z, S5v, Sha, Spd, Shv, T	0,911	0,844	0,878
Spk, Sk, S10z, S5v, Sha, Spd, Shv, S5p, T	0,900	0,854	0,877
Spk, Sk, S10z, S5v, Sha, Spd, Shv, S5p, Sdv, T	0,930	0,874	0,902
Spk, Sk, S10z, S5v, Sha, T, N_{av}	0,924	0,855	0,890
Spk, Sk, S10z, S5v, Sha, Spd, T, N_{av}	0,900	0,862	0,881
Spk, Sk, S10z, S5v, Sha, Spd, Shv, T, N_{av}	0,930	0,857	0,894
Spk, Sk, S10z, S5v, Sha, Spd, Shv, S5p, T, N_{av}	0,823	0,824	0,824
Spk, Sk, S10z, S5v, Sha, Spd, Shv, S5p, Sdv, T, N_{av}	0,870	0,855	0,863
Spk, Sk, S10z, S5v, T, N_{av}, K_d	0,934	0,863	0,899
Spk, Sk, S10z, S5v, Sha, T, N_{av}, K_d	0,864	0,874	0,869
Spk, Sk, S10z, S5v, Sha, Spd, T, N_{av}, K_d	0,942	0,866	0,904
Spk, Sk, S10z, S5v, Sha, Spd, Shv, T, N_{av}, K_d	0,923	0,877	0,900
Spk, Sk, S10z, S5v, Sha, Spd, Shv, S5p, T, N_{av}, K_d	0,845	0,859	0,852
Spk, Sk, S10z, S5v, Sha, Spd, Shv, S5p, Sdv, T, N_{av}, K_d	0,867	0,854	0,861
Spk, Sk, S10z, T, N_{av}, K_d, f_T	0,933	0,873	0,903
Spk, Sk, S10z, S5v, T, N_{av}, K_d, f_T	0,929	0,844	0,887
Spk, Sk, S10z, S5v, Sha, T, N_{av}, K_d, f_T	0,871	0,854	0,863
Spk, Sk, S10z, S5v, Sha, Spd, T, N_{av}, K_d, f_T	**0,928**	**0,885**	**0,907**
Spk, Sk, S10z, S5v, Sha, Spd, Shv, T, N_{av}, K_d, f_T	0,914	0,846	0,880
Spk, Sk, S10z, S5v, Sha, Spd, Shv, S5p, T N_{av}, K_d, f_T	0,882	0,848	0,865
Spk, Sk, S10z, S5v, Sha, Spd, Shv, S5p, Sdv, T, N_{av}, K_d, f_T	0,924	0,856	0,890
Spk, Sk, T, N_{av}, K_d, f_T, *v*	0,918	0,854	0,886
Spk, Sk, S10z, T, N_{av}, K_d, f_T, *v*	0,918	0,820	0,869
Spk, Sk, S10z, S5v, T, N_{av}, K_d, f_T, *v*	0,932	0,837	0,885
Spk, Sk, S10z, S5v, Sha, T, N_{av}, K_d, f_T, *v*	0,932	0,854	0,893
Spk, Sk, S10z, S5v, Sha, Spd, T, N_{av}, K_d, f_T, *v*	0,902	0,852	0,877
Spk, Sk, S10z, S5v, Sha, Spd, Shv, T, N_{av}, K_d, f_T, *v*	0,906	0,881	0,894
Spk, Sk, S10z, S5v, Sha, Spd, Shv, S5p, T, N_{av}, K_d, f_T, *v*	0,852	0,844	0,848
Spk, Sk, S10z, S5v, Sha, Spd, Shv, S5p, Sdv, T, N_{av}, K_d, f_T, *v*	0,932	0,872	0,902
Spk, T, N_{av}, K_d, f_T, *v, Mp/N*	0,874	0,860	0,867
Spk, Sk, T, N_{av}, K_d, f_T, *v, Mp/N*	0,929	0,839	0,884
Spk, Sk, S10z, T, N_{av}, K_d, f_T, *v, Mp/N*	0,922	0,872	0,897
Spk, Sk, S10z, S5v, T, N_{av}, K_d, f_T, *v, Mp/N*	0,912	0,837	0,875
Spk, Sk, S10z, S5v, Sha, T, N_{av}, K_d, f_T, *v, Mp/N*	0,924	0,861	0,893
Spk, Sk, S10z, S5v, Sha, Spd, T, N_{av}, K_d, f_T, *v, Mp/N*	0,918	0,857	0,888
Spk, Sk, S10z, S5v, Sha, Spd, Shv, T, N_{av}, K_d, f_T, *v, Mp/N*	0,924	0,871	0,898
Spk, Sk, S10z, S5v, Sha, Spd, Shv, S5p, T, N_{av}, K_d, f_T, *v, Mp/N*	0,864	0,843	0,854
Spk, Sk, S10z, S5v, Sha, Spd, Shv, S5p, Sdv, T, N_{av}, K_d, f_T, *v, Mp/N*	0,841	0,845	0,843

Based on the analysis of the results presented in Table 3, it was found that the values of the linear correlation coefficient for the learning and testing processes of the artificial neural network with principal component analysis and input parameters *Spk*, *Sk*, *S10z*, *S5v*, *Sha*, *Spd*, *T*, N_{av}, K_d and f_T are $R = 0{,}928$ for learning and $R = 0{,}885$ for testing. Moreover, the mean value of both processes is $R = 0{,}907$ and is the highest of those considered. The structure of the artificial neural network with principal component analysis for this variant is given in Figure 2.

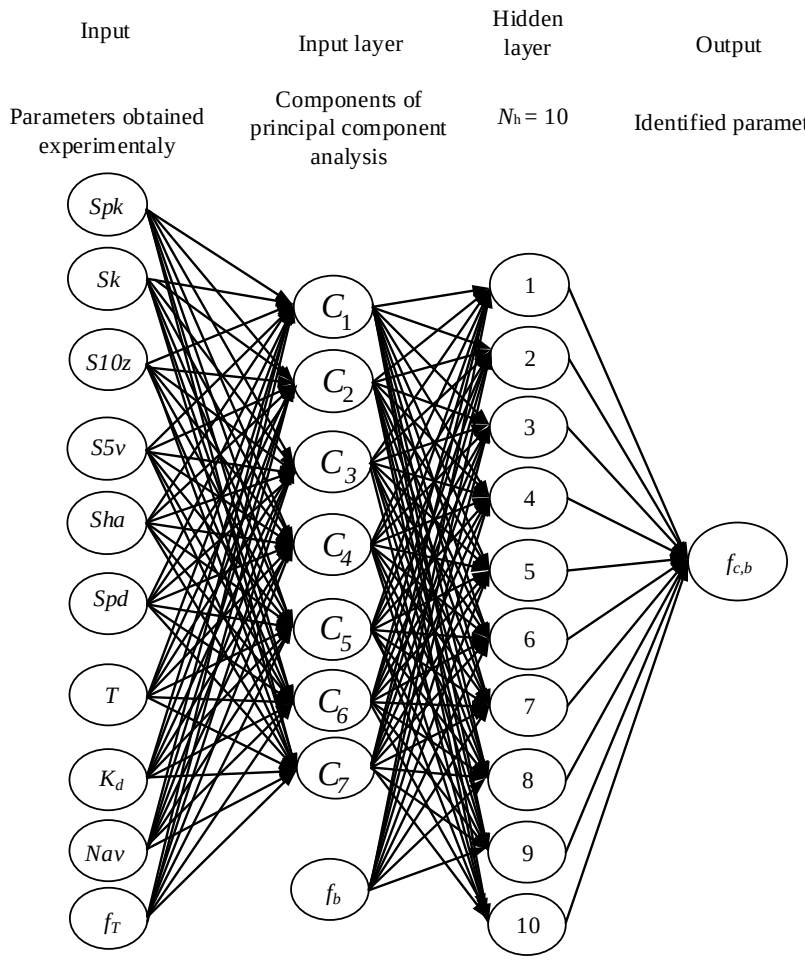

Fig. 2. Structure of the artificial neural network multilayer perceptron with principal component analysis

Figure 3 shows the relation between the pull-off adhesion $f_{c,b}$ value identified using the artificial neural network with principal component analysis, and the f_b value obtained from experimental tests using the pull-off method for the learning and testing processes.

Based on Figure 3, it was found that the artificial neural network with principal component analysis very accurately identifies the training data and also correctly identifies the testing data. This can be seen by the location of points along the regression line, corresponding to the ideal mapping and the obtained very high values of the linear correlation coefficient *R*, which are 0,928 for learning and 0,885 for testing.

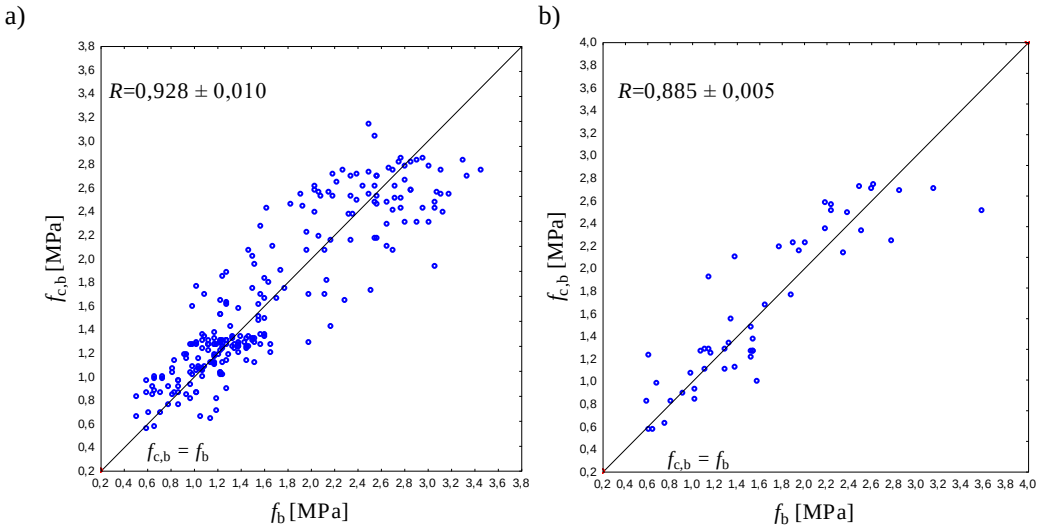

Fig. 3. Relation between the pull-off adhesion $f_{c,b}$ value identified using the artificial neural network with principal component analysis, and the f_b value obtained from experimental tests using the pull-off method for processes (a) learning and (b) testing

4. Conclusions

Based on the conducted research and numerical analysis, it was proved that identification of the interlayer bonding of concrete layers - the repair layer of variable thickness and the substrate layer - may be performed using complementary non-destructive methods and an artificial neural network with principal component analysis. It was shown that parameters describing substrate surface morphology obtained using the three-dimensional scanning laser method, parameters describing the thickness of the repair overlay, and parameters obtained using acoustic methods on the surface of the repair overlay are useful for this purpose. It was also shown that the artificial neural network with principal component analysis, learning algorithm Broyden-Fletcher-Goldfarb-Shano, 10 input parameters and 10 hidden layer neurons is most efficient for this purpose. This was proved by the very high value of the linear correlation coefficient for the learning process of R=0,928, as well as the high value for the testing process of R=0,885.

The presented method of identifying the pull-off adhesion value can be used in practice. This is due to the fact that it allows testing in any number of places without damaging the repair overlay. For this purpose, it is reasonable to perform verification on real objects.

References

[1] L. Czarnecki, P. Łukowski, A. Garbacz, Naprawa i ochrona konstrukcji z betonu – komentarz do PN-EN 1504 (in Polish), PWN, Warszawa 2017.
[2] PN-EN 1504 – 3:2006 Products and systems for the protection and repair of concrete structures - Definitions, requirements, quality control and evaluation of conformity - Part 3: Structural and non-structural repair. (in Polish), PKN, Warsaw 2006.
[3] M. Lukovic, Influence of interface and strain hardening cementitious composite properties on the performance of concrete repairs, PhD dissertation, TUDelft, 2016.
[4] Santos P., Julio E., Factors affecting bond between new and old concrete, ACI Materials Journal, vol. 108(4) (2011) s. 449-456.
[5] B. Bissonnette, L. Courard, A. Garbacz. Concrete Surface Engineering, CRC Press, Boca Raton 2017.
[6] J. Hoła, L. Runkiewicz, Methods and diagnostic techniques used to analyse the technical state of reinforced concrete structures, Structure and Environment 4 (2018) 309-337. https://doi.org/10.30540/sae-2018-030
[7] T.G. Mathia, P. Pawlus, M. Wieczorwski, Recent trends in surface metrology, Wear 271 (2011) 494-508. https://doi.org/10.1016/j.wear.2010.06.001
[8] S. Czarnecki, Non-destructive evaluation of the bond between a concrete added repair layer with variable thickness and a substrate layer using ANN, Procedia Engineering 172 (2017) 194-201. https://doi.org/10.1016/j.proeng.2017.02.049
[9] Ł. Sadowski, Adhesion in Layered Cement Composites, Springer Nature Switzerland, Cham 2019.
[10] I. Jolliffe, Principal component analysis, Springer Berlin Heidelberg, 2011.
[11] A. Herve, J. Lynne, Principal component analysis, wiley interdisciplinary reviews: computational statistics 2.4 (2010) 433-459.
[12] R. Fletcher, Practical methods of optimization. New York: John Wiley & Sons 1988.